An Accurate Retrieval of Cloud Droplet Effective Radius for Single-Wavelength Cloud Radar

Jiajing Du, Jinming Ge, Chi Zhang, Jing Su, Xiaoyu Hu, Zeen Zhu, Qinghao Li, Jianping Huang, and Qiang Fu

***Abstract*— The cloud droplets effective radius is a key feature that plays a critical role in influencing cloud microphysical processes and radiative effects. Accurate quantification of cloud effective radius (CER) is essential for advancing our understanding of cloud microphysics, refining cloud parameterization, and improving future climate prediction. Nonetheless, the accuracy of current CER retrieval algorithms, particularly relying on millimeter-wavelength cloud radar, is often largely affected by assumptions about the cloud droplet number concentration, inappropriate empirical coefficients, attenuated radar reflectivity, and limitations of other auxiliary instruments. In this study, we developed a novel CER retrieval algorithm for single-wavelength radar by leveraging the interconnections between CER, liquid water content (LWC), and cloud radar reflectivity. Unlike the previous studies, we first derive the LWC from a self-consistent method based on cloud liquid water mass absorption instead of empirical relationships. Subsequently, we correct the radar measured reflectivity attenuated by cloud water and perform sensitivity analysis to select an optimal parameter that minimizes the uncertainty associated with the given cloud droplet size distribution (DSD) assumption. Then, the CER is calculated from the retrieved LWC, corrected reflectivity, and the optimal parameter. We compared the frequency distribution, vertical structure, and error fraction of the retrieved CER with aircraft in situ measurements. Our results demonstrate higher consistency with in situ data compared to traditional empirical algorithms. Furthermore, the cloud optical thickness (COT) derived from the CER shows a much better agreement with Moderate Resolution Imaging Spectroradiometer (MODIS) products, which provides additional validation for the efficacy of our method in investigating cloud microphysical properties.**

***Index Terms*— Cloud effective radius (CER), cloud optical thickness (COT), cloud radar, retrieval method, self-consistent.**

Manuscript received 26 March 2024; revised 29 July 2024; accepted 16 August 2024. Date of publication 21 August 2024; date of current version 3 September 2024. This work was supported in part by the National Natural Science Foundation of China under Grant 42275076 and Grant 91937302, in part by the Science and Technology Project of Gansu Province under Grant 22JR5RA446, in part by the Fundamental Research Funds for the Central Universities under Grant lzujbky-2022-ct06, and in part by the Excellent Graduate Student "Innovation Star" Project of Gansu Province under Grant 2023CXZX-102. *(Corresponding author: Jinming Ge.)*

Jiajing Du, Jinming Ge, Chi Zhang, Jing Su, Qinghao Li, and Jianping Huang are with the Key Laboratory for Semi-Arid Climate Change of the Ministry of Education and College of Atmospheric Sciences, Lanzhou University, Lanzhou 730000, China (e-mail: gejm@lzu.edu.cn).

Xiaoyu Hu is with Chongqing Research Institute of Big Data, Chongqing 400041, China, and also with the School of Mathematical Sciences, Peking University, Beijing 100871, China.

Zeen Zhu is with the Environmental and Climate Sciences Department, Brookhaven National Laboratory, Upton, NY 11973 USA.

Qiang Fu is with the Department of Atmospheric Sciences, University of Washington, Seattle, WA 98105 USA.

Digital Object Identifier 10.1109/TGRS.2024.3447002

I. Introduction

CLOUDS cover approximately 60%–70% of Earth's surface, exerting a substantial effect on the energy budget of the Earth–atmosphere system by modulating both solar and terrestrial radiation. They also play a pivotal role in the transport of moisture and the distribution of water through processes such as condensation and precipitation, which further results in the regulation of the hydrological cycle, atmospheric circulation, and, subsequently, the shaping of climate patterns [1], [2], [3], [4]. Low-level clouds (LLCs), prevalent at altitudes typically below 2–3 km height, have strong mitigation effects on global warming by reflecting incoming solar radiation [5], [6]. The radiative effect of LLCs on our climate is largely determined by their specific physical properties. Even minor changes in properties will significantly impact on both short-term weather pattern and long-term climate change [7], [8], [9]. Furthermore, understanding the vertical distribution of microphysical properties provides insights into the dynamic and thermal processes that ultimately controlling cloud development and life cycle [10]. In the context of global warming, the intensified processes of condensation, evaporation, and phase transition will invariably modify the properties of LLCs. These alterations will in turn influence climate energy balance, which is known as the cloud feedback mechanisms, constituting one of the primary sources of uncertainties in future climate predictions [11]. Therefore, the endeavor to accurately characterize LLC properties holds significant implications for enhancing our predictive capabilities in understanding, and anticipating the impacts of climate change [12], [13].

Cloud droplet size is one of the key LLC features that not only determines cloud optical quantities such as cloud single scattering albedo but also exerts influence over the cloud–aerosol interaction and serves as a reflection of their interdependence [14], [15], [16], [17]. For instance, under a fixed liquid water path (LWP), smaller droplet sizes can reflect more solar radiation back to space and prolong cloud life by reducing precipitation efficiency. Previous studies have proven that a reduction in cloud droplet size of approximately 15%–20% (e.g., approximate size reduction of 2 μm for 10-μm cloud droplets) would offset the warming effect induced by doubling CO_2 in the atmosphere [18]. Cloud effective radius (CER, r_e), which takes into account individual cloud particle cross-sectional area and the total particle concentrations in a cloud layer, represents the average size of the cloud droplets. It is listed as one of the essential climate variables (ECVs) by the global climate observing system (GCOS) for investigation of global climate change [19], [20]. The cloud physical processes and radiative effects incorporated in climate models are largely governed by the CER vertical evolutions [21]. Therefore, accurately obtaining cloud droplet size profiles is of great significance in enhancing cloud parameterization in models for future climate predictions.

Various algorithms, employing both passive (e.g., microwave radiometer (MWR), visible, infrared, and multispectral imagers) and active (e.g., radar and lidar) remote sensing instruments, either independently or in combination, have been developed for CER retrieval [22], [23], [24]. The widely adopted approach involves inferring CER from passive instruments by capturing reflected solar radiation from clouds through single channel or multichannel, enabling the investigation of large-scale global cloud properties. However, accurately deriving vertical profiles of CER using passive instruments remains challenging due to their limitation in observing information solely at the cloud top [25]. In contrast, cloud radar operating at a millimeter wavelength has the capability to penetrate thick cloud and is a powerful instrument for revealing high-resolution cloud vertical structures [26]. Since cloud radar reflectivity (Z) is proportional to the sixth moment of the cloud droplet size distribution (DSD) and CER is the ratio of the third to the second moment of the DSD, several methods have been developed to establish a linkage between CER and radar measured reflectivity (Z_m, in unit of dBZ). These approaches are primarily classified into three categories: traditional empirical methods [27], [28], optimal retrieval algorithms with lookup tables [29], and joint retrieval methods combining other cloud microphysical variables from passive instruments [30], [31]. Traditional empirical methods derive coefficients either by directly fitting the in situ and radar observations or by assuming a certain DSD with some constant parameters such as the cloud number concentration N_T, spectral width σ_x, and the order β in lognormal and gamma distribution [32], [33], [34]. However, limitations arise due to the scarcity and high cost of in situ measurements, as well as discrepancies between assumed constant parameters and the diverse range observed in actual data. For example, a previous study has shown that the real N_T has a significant vertical structure that increases and then decreases with altitude [35]. Optimal retrieval algorithms are constrained to specific cloud conditions with prior lookup table data, depending on accurate cloud parameterization in numerical models. The intricate calculation process adds complexity and uncertainty to the optimal algorithm. Multi-instruments joint algorithms, while effective in reducing retrieval uncertainties through constraints from other properties, are influenced by spatiotemporal mismatches and distinct sampling accuracies among various sensors. Given these challenges, it is crucial to develop an algorithm capable of overcoming current limitations without relying on additional instruments and ultimately ensuring a robust and versatile approach for CER retrieval in diverse cloud conditions.

In this study, we propose a novel method to retrieve CER for single-wavelength cloud radar, which is independent of the N_T assumption, empirical coefficients, and other instruments. The whole method includes establishing the expressions of CER with Z, liquid water content (LWC), and cloud DSD parameters attributed to their physical definitions, performing sensitivity analysis of factors related to cloud DSD parameter, and obtaining self-consistent LWC and unattenuated reflectivity (Z). Here, the DSD is assumed to follow lognormal distribution, which has been demonstrated to provide a suitable representation for the wide range of droplet sizes typically encountered in atmospheric clouds. The DSD parameter is optimally selected by a sensitivity analysis to minimize its impact on retrieval results. The LWC is retrieved from a self-consistent method based on cloud liquid water mass absorption without the incorporation of empirical coefficients and other instruments apart from cloud radar [36]. Z_m is also corrected simultaneously following the proportional function between LWC and absorption attenuation. The data and instruments used for the method evaluation and the details of method are introduced in Sections II and III, respectively. The feasibility and accuracy of the method are evaluated in Section IV by applying it to the ground-based cloud radar and comparing the results with aircraft in situ data. Moreover, the reliability of our algorithm in cloud optical properties retrieval is further assessed by comparing the COT calculated from the retrieved CER with moderate resolution imaging spectroradiometer (MODIS) products, as discussed in Section V before the conclusion drawn in Section VI.

II. Instrument and Dataset

The Eastern North Atlantic (ENA; 39.09°N and 28.02°W) site, established and operated by the U.S. Department of Energy (DOE) Atmospheric Radiation Measurement (ARM) Program, is a critical site for probing cloud properties in the mid-latitude marine environment since it is located in the Atlantic Ocean with widely distributed LLCs [37]. The Ka-band zenith radar (KAZR) operated at 35 GHz receives backscatter echoes in dual-polarization modes and provides Doppler velocity, Doppler spectrum width, and co- and cross-polarized radar reflectivity factor by calculating the first three moments of the radar Doppler spectra [38], [39]. The active remote sensing of clouds (ARSCL) value-added product (VAP) derived from the combination of KAZR, Vaisala laser ceilometer (CEIL), and micro-pulse lidar (MPL) provides cloud vertical structure with 4s and 30-m temporal and spatial resolutions, where the hydrological echoes are distinguished from KAZR background noise and nonhydrological signals, and the cloud base height (CBH) is determined through the combination of CEIL and MPL at a wavelength of 532 nm [40], [41].

The aerosol and cloud experiments in the ENA (ACE-ENA) field campaign were carried out at the ENA site from June 2017 to February 2018 [42]. During the ACE-ENA field campaign, there are two intensive observation periods (IOPs) in summer (from June 21 to July 20, 2017) and winter (from January 15 to February 18, 2018). The ARM aerial facility (AAF) Gulfstream-159 (G1) research aircraft, flying 20 and 19 missions in the summer and winter IOPs, respectively, provides multiple products of the marine boundary layer (MBL) cloud microphysical properties [43]. The fast cloud droplet probe (FCDP) mounted on the G1 aircraft is an essential instrument for measuring the number concentration and size of hydrometeor particles ranging from 1 to 50 μm, with a particle size resolution of approximately 3 μm and a temporal resolution of 1 s [44], [45].

The radar measured reflectivity factor provided by the ARSCL VAP during the summer and winter IOPs in the ACE-ENA campaign is used as the inputs of the retrieval algorithm. The cloud boundaries are jointly determined by the CBH derived from ARSCL VAP and the cloud top height (CTH) identified from the KAZR cloud echoes. The radar profiles with CBH lower than 3 km and CTH lower than 4 km are selected as cloud layers dominated by liquid water droplets. The CER produced by FCDP less than 16 μm is utilized for verifying and assessing the applicability and uncertainty of the retrieval algorithm. Simultaneously, with the aim of minimizing the spatial and temporal matching discrepancies between aircraft measurement and radar detection, thereby utilizing aircraft data to assess CER retrieval errors, only the in situ data within 10 km from the ENA site are used in this study. In addition, the cloud optical thickness (COT) products from the MODIS observations with the resolution of 1 × 1 km (i.e., MOD06 and MYD06) are used for validating the efficiency of our method in COT retrieval, where MOD06 and MYD06 are the Level 2 cloud products from MODIS onboard the Aqua and Terra satellites, respectively [46]. The MODIS COT within a 0.5° × 0.5° boxed area centered at the ENA site is selected to compare with the mean COT from this method within a 40-min window on MODIS overpass time, which is proved to be optimal for ground radar and spaceborne sensors comparisons from our previous studies [47], [48].

III. Retrieval Method

The CER is defined as the ratio of the third moment to the second moment of the cloud DSD shown as follows:

$$r_e = \frac{\int_0^\infty n(r) r^3 dr}{\int_0^\infty n(r) r^2 dr} = \frac{\langle r^3 \rangle}{\langle r^2 \rangle} \tag{1}$$

where r is the cloud droplet radius, $n(r)$ is the cloud DSD representing the number of cloud droplets with sizes in the range from r to $r + dr$ per unit volume, and $\langle r^l \rangle$ is the lth moment of the cloud DSD. The cloud DSD is commonly approximated by the lognormal distribution as expressed by [29]

$$n(r) = \frac{N_T}{\sqrt{2\pi} r \sigma_x} \exp\left[\frac{-\ln^2(r/r_m)}{2\sigma_x^2}\right] \tag{2}$$

where N_T is the total cloud droplet number concentration, r_m is the median radius, and σ_x is the logarithmic spectral width, which are defined as $r_m = \exp(\overline{\ln r})$ and $\sigma_x = \ln\left(\overline{(\ln r - \ln r_m)^2}\right)^{1/2}$. The lth moment of this distribution is $\langle r^l \rangle = r_m^l \exp((l^2/2)\sigma_x^2)$, and hence, the CER in (1) can be further rewritten as

$$r_e = r_m \exp\left(\frac{5}{2}\sigma_x^2\right). \tag{3}$$

Note that the Z and cloud LWC can be expressed as

$$Z = \int_0^\infty n(r) r^6 dr = 64 N_T r_m^6 \exp\left(18\sigma_x^2\right) \tag{4}$$

$$\mathrm{LWC} = \int_0^\infty \rho_w n(r) \frac{4}{3}\pi r^3 dr = \frac{4}{3}\pi N_T \rho_w r_m^3 \exp\left(\frac{9}{2}\sigma_x^2\right) \tag{5}$$

which are both closely associated with the cloud DSD parameters r_m and σ_x^2. According to these definitions, the relationship between r_m and $\exp(\sigma_x^2)$ can be established by eliminating N_T through the combination of (4) and (5) as

$$r_m^3 \exp\left(\frac{27}{2}\sigma_x^2\right) = \frac{\pi\rho}{48}\frac{Z}{\mathrm{LWC}}. \tag{6}$$

r_m and σ_x can be expressed as functions of LWC and Z from (6), and thus, the CER can be rewritten either as a function of parameter r_m or σ_x in conjunction with radar reflectivity Z and cloud LWC as shown in the following two equations:

$$r_e = \left(\frac{\pi\rho}{48}\frac{Z}{\mathrm{LWC}}\frac{1}{\exp\left(6\sigma_x^2\right)}\right)^{\frac{1}{3}} \tag{7}$$

$$r_e = r_m^{\frac{4}{9}}\left(\frac{\pi\rho}{48}\frac{Z}{\mathrm{LWC}}\right)^{\frac{5}{27}}. \tag{8}$$

While both equations can be used for the derivation of CER, it is essential to note their dependence on the assumption that the DSD parameter (σ_x or r_m) remains constant. Consequently, it is imperative to assess the sensitivity of (7) and (8) with respect to the parameter changes to determine which one is less affected by the parameter variation and can yield more reliable results. Two crucial aspects are sequentially addressed. First, we conduct a sensitivity test to examine the impact of parameter variations on the retrieved results and select the equation with less sensitive to parameter changes. The appropriate value of the parameter in the chosen equation is assigned from the most reasonable and widely accepted values in the literature. Second, we obtain accurate LWC by incorporating adaptive constraints on physical processes related to cloud liquid water absorption attenuation and correct the Z_m using the LWC. Thus, we propose a self-consistent algorithm consisting of these two primary steps for retrieving CER, and the details are illustrated in the flowchart, as depicted in Fig. 1.

A. Sensitivity Analysis and Optimal Parameter Selection

In order to select the optimal parameter for CER retrieval, we conducted sensitivity tests on σ_x and r_m, independently through the ratio of the CER changes, arising from parameter amplification by a factor of $\boldsymbol{k}$ to the originally retrieved CER. The parameter sensitivities of σ_x and r_m shown in (7) and (8) can be expressed as follows:

$$\frac{\Delta r_e}{r_e} = \exp\left[2\sigma_0^2(1 - \boldsymbol{k}^2)\right] - 1 \tag{9}$$

$$\frac{\Delta r_e}{r_e} = \boldsymbol{k}^{\frac{4}{9}} - 1 \tag{10}$$

where $\boldsymbol{k}$ denotes the multiplier by which the parameter is either increased ($\boldsymbol{k} > 1$) or reduced ($0 < \boldsymbol{k} < 1$). σ_0 in (9) represents the parameter σ_x before being modified by a factor of $\boldsymbol{k}$ with a

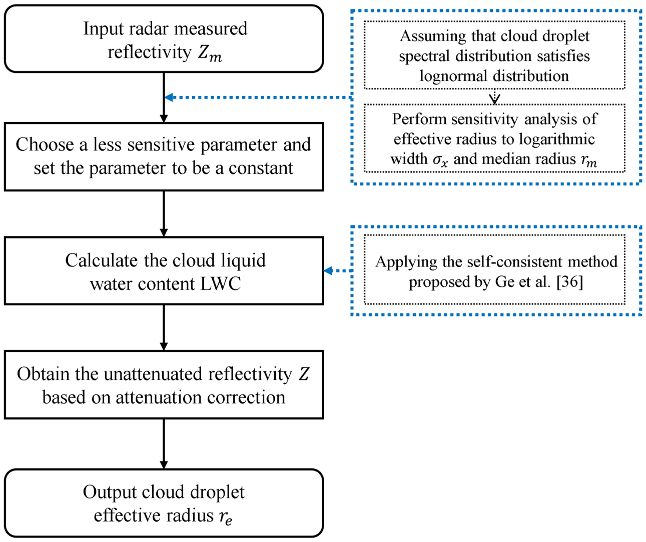

Fig. 1. Flowchart of the CER retrieval by our method. The framework of the overall algorithm is shown on the left and the method used to compare the sensitivity of the algorithm for different parameters and calculate the cloud LWC is shown in the blue dashed box on the right.

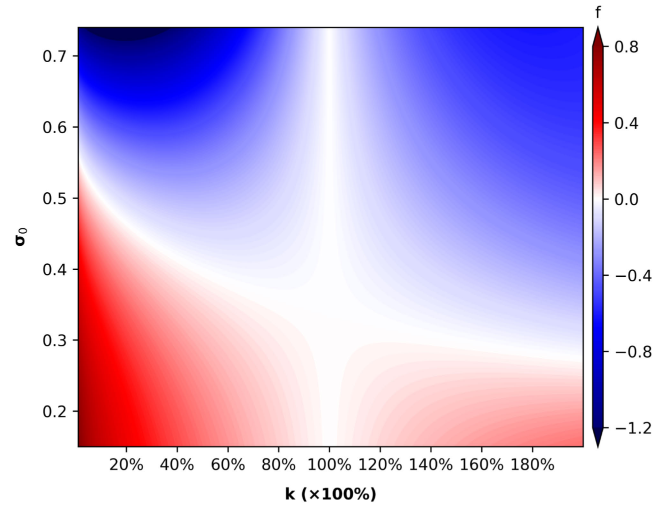

Fig. 2. Comparison of algorithm sensitivity to variations in parameters σ_x and r_m. $\boldsymbol{k}$ and σ_0 are the percentage by which the parameters are amplified or reduced and the initial value of σ_x, respectively. The value of $\boldsymbol{k}$ equal to 100% represents that the parameter value remains unchanged, without any enlargement or reduction.

value within the range of 0.15–0.74. This range is referenced in numerous previous studies on DSD parameters as summarized by Miles et al. [49]. Remarkably, r_m in (10) cancels out as it is equal in both the numerator and denominator, resulting in an independence of sensitivity to the changes in r_m. Consequently, the influence of σ_x variation on the retrieved results is contingent upon its initial value σ_0. Conversely, the sensitivity is independent of the r_m initial value. To quantify the relative sensitivity of different parameters, we further compare the absolute sensitivity differences induced by variations in the r_m and σ_x parameters as follows:

$$f = \left|\boldsymbol{k}^{\frac{4}{9}} - 1\right| - \left|\exp\left[2\sigma_0^2\left(1-\boldsymbol{k}^2\right)\right] - 1\right|. \tag{11}$$

The f values correspond to distinct percentages of $\boldsymbol{k}$ for varying σ_0, which are shown in Fig. 2. A negative value of f means that the retrieved CER variation resulting from alteration of r_m by a factor of $\boldsymbol{k}$ is less significant than that of σ_x and vice versa. For example, taking an average σ_0 value of 0.38 for marine cloud from previous studies and a $\boldsymbol{k}$ of 1.2 corresponding to the horizontal axis 120% (i.e., both r_m and σ_x increase by 20%), the f value is -0.035, indicating that the CER variation caused by a 20% increase in r_m is smaller than it caused by the same percentage variation of σ_x. It can be seen that the algorithm is less sensitive to the parameter σ_x when σ_0 is smaller than 0.28, as indicated by the positive f values within this range. However, f is gradually dominated by a negative value with the increase of σ_0. Especially when σ_0 is greater than 0.56, the retrieved results variations caused by the r_m changes are smaller than that of σ_x no matter the parameter is reduced or expanded. Namely, the algorithm is less sensitive to a given constant r_m and the sensitivity of σ_x demonstrates a pronounced dependence on σ_0. Therefore, it is optimal to choose (8) in which the results are less affected by the parameter r_m assumption. Here, the value of 13.1 μm is adopted in our method as the constant r_m based on the average value of marine clouds from previous studies [49]. We also calculate the retrieved results under the assumption of other arbitrary r_m values. It is found that the change in CER is caused by the variation of r_m within the standard deviation range (i.e., 13.1 ± 3.6 μm) is merely 11%.

B. LWC Retrieval and Radar Reflectivity Attenuation Correction

According to (8) selected through parameter sensitivity analysis, the CER retrieval is inseparable from accurate LWC and unattended radar reflectivity Z in addition to r_m. Thereby, we utilize a self-consistent cloud LWC retrieval algorithm developed from our previous study [36] to calculate LWC and correct the absorption attenuation on Z_m using the radar equation presented later.

The LWC retrieval algorithm is constructed based on the interdependencies between cloud physical variables without relying on any other instruments and empirical coefficients. Specifically, the proportional relationship between absorption attenuation coefficient A and LWC (i.e., $A = K^*\text{LWC}$) regardless of DSD under the Rayleigh approximation is utilized in LWC retrieval. Considering that the disparity between Z_m and Z is determined by the LWC and the relationship among Z_m, Z, and LWC can be expressed as the radiative transfer equation of $Z = Z_m 10^{-0.2\int A(s)ds}$ (i.e., radar equation), we convert this radar equation into the Bernoulli differential equations (BDEs) and integrate it within the cloud layer to explore the LWC at a point where the relationships among the variables achieve self-consistency [36]. The proportional coefficient K^* is related to the radar wavelength, temperature, and complex refractive index of cloud droplets with the unit of dB km^{-1}. It can be regarded as a constant for a cloud radar operating at a fixed millimeter wavelength. Therefore, the optimal parameters in LWC expression within each radar range can be obtained by minimizing the error between Z_m and theoretically reconstructed reflectivity factor expressed by

LWC through the trust region reflective (TRR) method. The algorithm accuracy has been substantiated by comparing the retrieved LWC with aircraft in situ data and MWR products. Both of them showed that the LWC retrieved by this method has significant improvements for both single-layer and multi-layer clouds, especially mitigating the overestimation of large particle clouds caused by traditional empirical relationships.

C. Algorithm Uncertainty Analysis

From (8), one can see that the CER retrieval uncertainty is determined by Z, LWC, and r_m. Therefore, we analyze the retrieval uncertainty by calculating the relative error as expressed by [50]

$$\frac{\Delta \mathrm{CER}}{\mathrm{CER}} = \pm\left[\left(\frac{5\Delta Z}{27Z}\right)^2 + \left(\frac{5\Delta \mathrm{LWC}}{27\mathrm{LWC}}\right)^2 + \left(\frac{4\Delta r_m}{9r_m}\right)^2\right]^{\frac{1}{2}} \tag{12}$$

where ΔZ, ΔLWC, and Δr_m are the radar reflectivity uncertainty in ± 1 dBZ [41], the standard deviation of retrieved LWC in ± 0.1 g m^{-3} [36], and the r_m standard deviation in ± 3.6 μm as proposed by Miles et al. [49], respectively. Z, LWC, and r_m represent the radar reflectivity for nonprecipitating clouds, the average of retrieved LWC in 0.2 g m^{-3} [36], and the mean value of r_m in 13.1 μm, respectively [49]. Considering that Z is in the range of -40 to -10 dBZ for nonprecipitating clouds, we assume Z as -30 dBZ and calculate the CER uncertainty by applying (12). The result shows that the uncertainty is 15.3%, which is less than 16.0% of the combined MWR and cloud radar algorithm proposed in previous studies [50]. In addition, we calculate the uncertainty for different reflectivity factors. It is found that the uncertainty varies only within 0.1% for the Z varying from -40 to -10 dBZ. Thus, the advantage of our method is that it not only provides CER products without using other instruments but also has lower uncertainty than previous retrieval algorithms.

IV. Results and Analysis

We applied this method to the ground-based Ka-band radar installed at the ENA site spanning over one year from June 2017 to May 2018 and separately compared its results with the CER, provided by aircraft in situ instruments and other retrieval methods during the entire IOPs. The application process of the method in cloud radar and the spatial–temporal matching of its results to aircraft in situ data are demonstrated by the nonprecipitation MBL cloud cases occurred on June 30, 2017 and January 29, 2018, respectively.

A. Case Study

Taking a single-layer MBL cloud that occurred on June 30, 2017 as an example, the retrieval process is concretely displayed in Fig. 3. This case is a typical stratocumulus with no obvious large particles below the CBH (KAZR measured CBH close to the CEIL detected CBH marked by black dots). As shown in Fig. 3(b), the cloud LWC derived from the self-consistent algorithm is concentrated below 0.4 g m^{-3} and increases significantly around 19:00 UTC prior to the

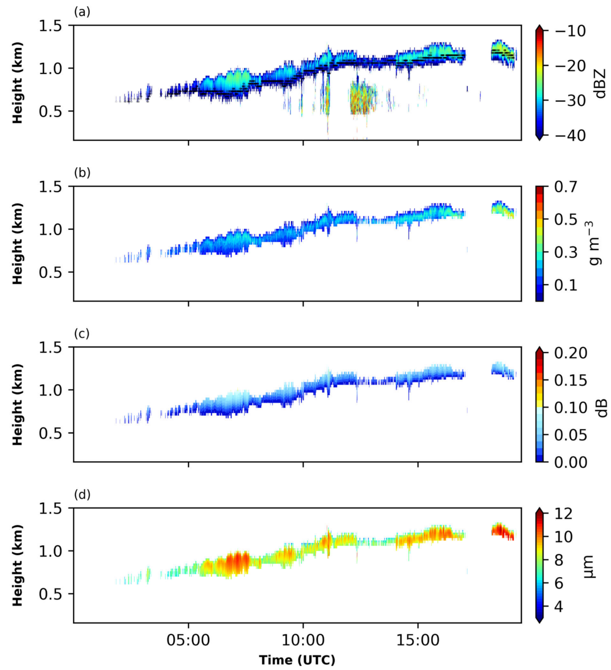

Fig. 3. Application of the algorithm to the single single-layer cloud case on June 30, 2017. Time–height profiles of (a) KAZR measured reflectivity factor identified from the background noise and low-level nonhydrographic signals, (b) retrieved cloud LWC, (c) difference between the unattended and measured reflectivity, and (d) CER retrieved by our method. The black dots marked in (a) are the best estimated CBH provided by the combination of CEIL and MPL.

precipitation. The differences between attenuation corrected and measured reflectivity are less than 0.2 dB [Fig. 3(c)]. This is consistent with the statement proposed by Yao et al. [51] that the Ka-band radar attenuation correction for nonprecipitating clouds is below 1 dB. Utilizing the calculated LWC and the corrected reflectivity, the CER retrieved by our method (hereafter $\mathrm{CER_{Ret}}$) is within the range of 6–12 μm, as shown in Fig. 3(d). The results are similar to the previous findings that the effective radius of MBL nonprecipitation clouds over the Azores is concentrated in the range of 6–14 μm [52].

The matchups between $\mathrm{CER_{Ret}}$ and CER provided by FCDP (hereafter $\mathrm{CER_{FCDP}}$) is exemplified by a nonprecipitation cloud case that occurred on January 29, 2018 as shown in Fig. 4, aiming to provide retrieval results from both summer and winter IOPs, respectively. The G1 aircraft track varying with longitude, latitude, and time is depicted by 2-D and 3-D graphs in Fig. 4(a) and (b), respectively. To ensure spatial consistency between aircraft and radar observation, we select the in situ data within 10 km from the ENA site and compare it with $\mathrm{CER_{Ret}}$ averaged over the three consecutive radar bins centered on the aircraft heights [53]. The altitudes of in situ data within the cloud layer are marked as magenta dots in Fig. 4(c) and the $\mathrm{CER_{FCDP}}$ values are indicated by blue dots in Fig. 4(d). It can be seen that $\mathrm{CER_{Ret}}$ [the red dots in Fig. 4(d)] follows the trend of $\mathrm{CER_{FCDP}}$ with a relatively smaller average value (11.02 ± 2.39 μm versus 11.79 ± 1.66 μm). The root-mean-square error (RMSE) is 2.74 μm by regarding $\mathrm{CER_{FCDP}}$ as the true value. Similar to what is demonstrated in this cloud case, the method accuracy is further statistically quantified by

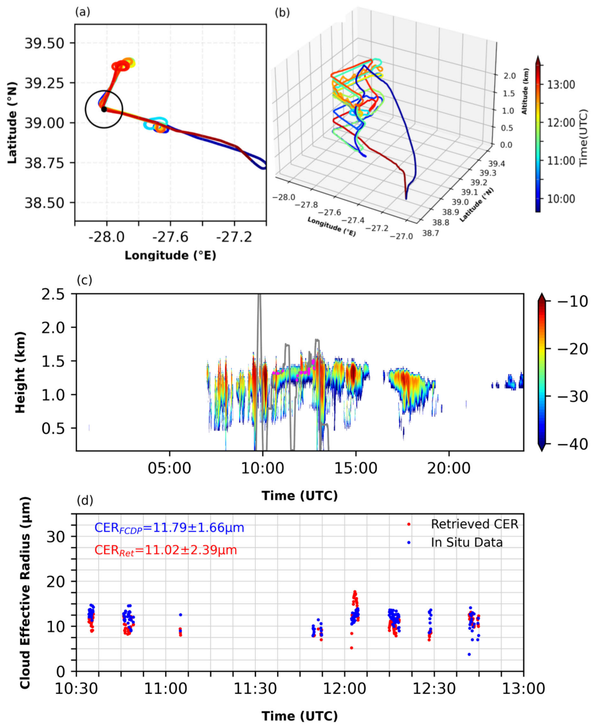

Fig. 4. (a) G1 aircraft track for cloud case occurred on January 29, 2018 during winter IOPs. The black circle is the boundary of 10 km from the ENA site. (b) 3-D schematic of the G1 aircraft flight altitudes at different times. The color bar on the right represents the universal time. (c) Time–height profiles of the KAZR measured reflectivity and the aircraft altitudes are marked by the gray dots. The data where the flight altitude is between the CBH and CTH as well as the distance from the ENA site is within 10 km are marked by magenta dots. (d) Comparison of the retrieved CER with the aircraft in situ data. The blue dots represent the CER_{FCDP} corresponding to the magenta dots in (c). The red line represents the averaged CER_{Ret} over the three consecutive radar bins centered on the aircraft heights of the magenta dots in (c).

comparing the retrieved results with aircraft in situ data from two IOPs during the ACE-ENA campaign in Section IV-B.

B. Statistical Analysis

To validate the rationality of parameter selection and estimate the method retrieval error, we compare the CER retrieved by distinct approaches with CER_{FCDP} during summer, winter, and entire IOPs. The different approaches used for assessment include the algorithm with constant parameter σ_x (hereafter CER_σ) as presented by (7), the traditional empirical method $CER = 22.7\exp^{(0.0384\,dBZ_e)}$ for winter IOPs, and $CER = 26.78\exp^{(0.0384\,dBZ_e)}$ for summer IOPs proposed by Dong et al. [34] (hereafter CER_{Tra}) and CER_{Ret}. The intercomparison of the CER derived from these methods with the in situ data and their frequency distributions are shown in Figs. 5 and 6, respectively. The CER retrieval errors are quantified through the mean bias (MB), RMSE, and fractional error (i.e., $|((CER - CER_{FCDP})/CER_{FCDP})| \times 100\%$) by taking the aircraft in situ data as true value. During the summer IOPs [Fig. 5(a1)–(c1)], CER_{Ret} values are consistent with CER_{FCDP} and have smaller MB (i.e., -0.39 μm versus -2.63 and -0.95 μm) and RMSE (i.e., 4.58 versus 6.95 and 4.94) than that of CER_σ and CER_{Tra}. The frequency distribution of

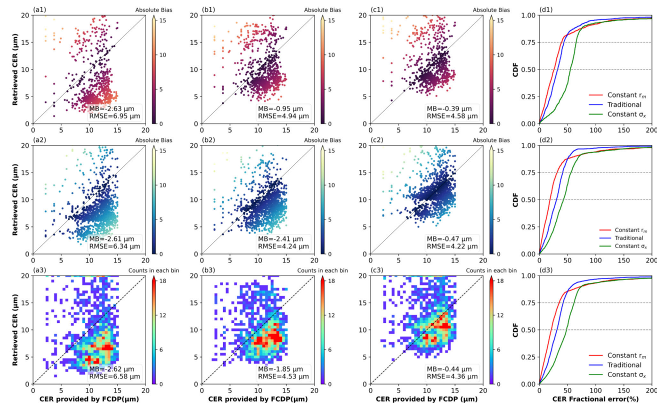

Fig. 5. Comparison of the CER retrieved by (a1)–(a3) algorithm with constant σ_x, (b1)–(b3) traditional empirical method and (c1)–(c3) algorithm with constant r_m proposed in this study with the CER provided by FCDP onboard the G1 aircraft during summer (the top panel), winter (the middle panel), and the entire IOPs (the bottom panel). The black dashed line at the diagonal position of the subgraph in three columns from left to right represents that the retrieved CER is the same as the CER_{FCDP}. The cdf of the CER fractional error for the algorithm with constant σ_x (green solid line), the traditional empirical method (blue solid line), and our method (red solid line) are shown in the fourth column (d1)–(d3), respectively. The gray dashed lines represent the cdf is equal to 0.5 and 0.75.

CER_{Ret} and CER_{FCDP} also has the proximate peaks (8.56 μm versus 10.78 μm), as shown in Fig. 6(a). Similar to the above comparisons, the retrieved results show smaller error than the other two algorithms both in winter [Fig. 5(a2)–(c2)] and the entire IOPs [Fig. 5(a3)–(c3)]. Specifically, the cumulative distribution functions (cdfs) of CER_{Ret} fractional error is on the leftmost side whether in summer [Fig. 5(d1)], winter [Fig. 5(d2)], and entire IOPs [Fig. 5(d3)]. This confirmed that the errors of our method are concentrated in a narrow range and CER_{Ret} are in good agreement with the aircraft in situ data. Moreover, the frequency distribution of CER_{FCDP} in winter IOPs [Fig. 6(b)] exhibits a similar distribution with peaks at 11.31 μm. Considering that the precipitation rate will increase in winter due to the stronger ability of aerosol particles to serve as cloud condensation nuclei, more frequent low-pressure systems bringing moist air masses and a less stable atmosphere associated with midlatitude cyclones than in summer [54], [55], [56], the CER_{Ret} distribution is still close to the peak of CER_{FCDP} even in the presence of precipitation. It is affirmed that our method can be applied to small cloud droplets with high accuracy and is less affected by large precipitation particles in clouds.

Given that the CER vertical distribution is also a pivotal property that reflects the condensation and coalescence growth of cloud droplets [57], we further classify CER_{Ret}, CER_σ, CER_{Tra}, and CER_{FCDP} according to their altitudes in a 0.3-km bin and analyze their mean and standard deviation errors in each altitude bin. As displayed in Fig. 7(a), the CER exhibits an ascending trend with altitudes irrespective of the approach employed. This aligns well with the statement proposed by Chen et al. [58] that the CER of nonprecipitation clouds dominated by condensation growth generally increases with altitudes. Moreover, it is obvious that the average values of the CER retrieved by different algorithms are smaller than

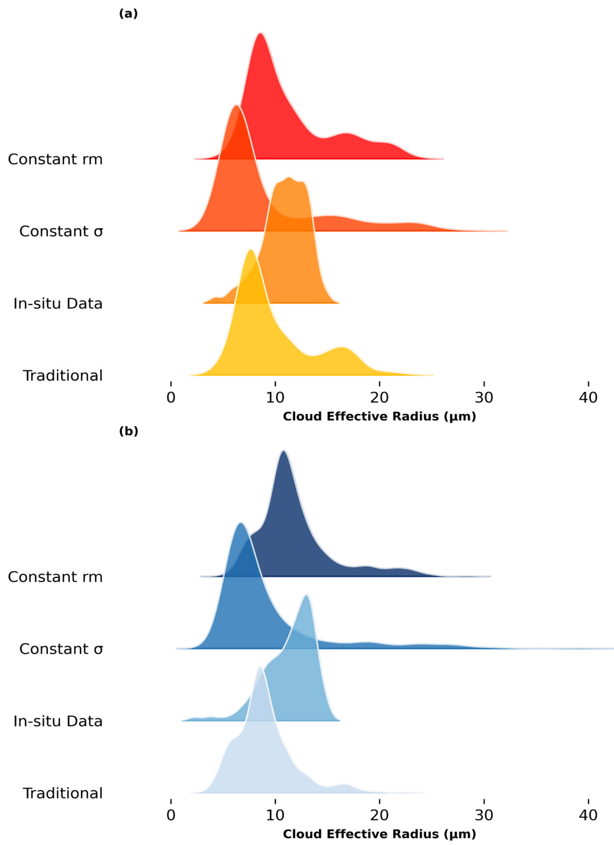

Fig. 6. Ridgeline plots showing the frequency distribution of the CER provided by different approaches during (a) summer and (b) winter IOPs. The CER derived from our method with constant r_m proposed in this study, the algorithm with constant σ_x, the in situ data, and the traditional empirical method are shown in each subgraph from top to bottom. The horizontal scale is aligned to be the same and the distribution plots overlap slightly for clarity.

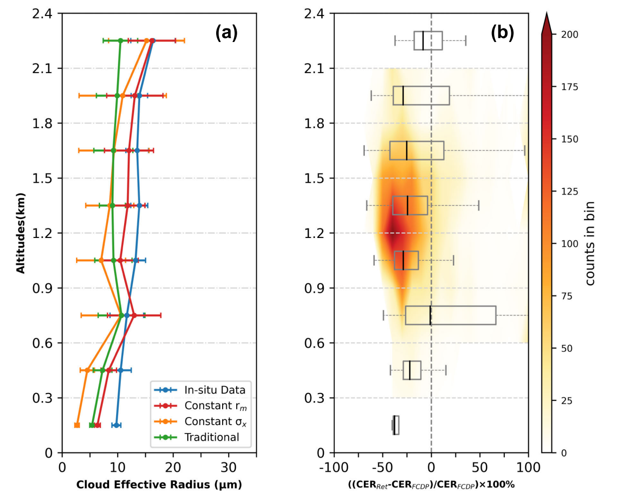

Fig. 7. Profiles of (a) CER provided by in situ data (blue solid line), the algorithm with constant r_m proposed in this study (red solid line), the algorithm with constant σ_x (yellow solid line), and the traditional empirical method (green solid line), and (b) fractional error of CER$_{\mathrm{Ret}}$ versus the altitude where the cloud echoes are located. The mean and the standard deviation of the different methods retrieved CERs within the altitudes bin of 0.3 km are shown as dots and error bars in (a), and CER$_{\mathrm{Ret}}$ fractional error distribution within each altitude bin is displayed by a gray boxplot in (b). The gray dashed line shown in (b) represents the fractional error is equal to zero.

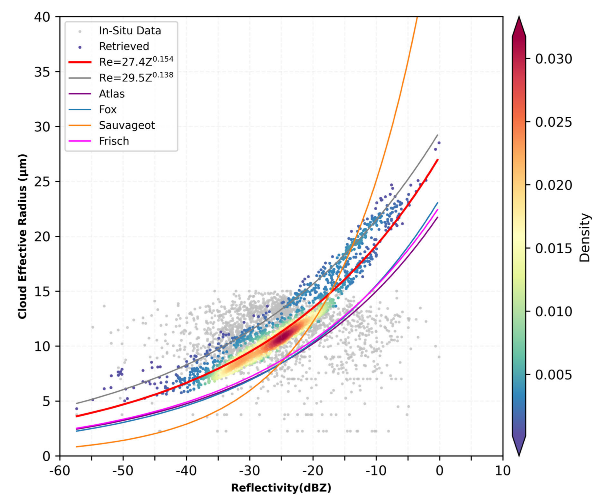

Fig. 8. Comparison of the line fit by CER$_{\mathrm{Ret}}$ and Z (red solid line) with the line fit based on in situ data (gray solid line) and other traditional empirical formulas, respectively. The gray and colored dots represent the CER provided by the aircraft and retrieved from our method, respectively. The density of CER$_{\mathrm{Ret}}$ is represented by the color bar as shown on the right.

that of in situ data, while CER$_{\mathrm{Ret}}$ exhibits higher consistency with CER$_{\mathrm{FCDP}}$ than that of CER$_{\sigma}$ and CER$_{\mathrm{Tra}}$. Furthermore, the error distributions for CER$_{\mathrm{Ret}}$ are depicted in Fig. 7(b). The median of CER$_{\mathrm{Ret}}$ absolute fractional error at the altitudes where the cloud echoes mainly concentrated (i.e., altitudes from 0.9 to 1.5 km) is within 50%, as shown by the box plots with the dark red area in Fig. 7(b), which further reveals that the retrieval error of our method is concentrated within a narrow variation range.

Aside from evaluating the method accuracy using one of the traditional empirical methods as illustrated above, we also compare the coefficients fit from CER$_{\mathrm{Ret}}$ and Z with various empirical coefficients proposed by distinct researchers in existing studies. For example, the traditional empirical methods proposed by Atlas [27] for nonprecipitating liquid clouds as $\mathrm{CER} = 22Z^{0.167}$, Sauvageot and Omar [59] for cumulus and stratocumulus clouds as $\mathrm{CER} = 51.5Z^{0.313}$, Frisch et al. [50] for marine stratocumulus clouds as $\mathrm{CER} = 22.7Z^{0.167}$, and Fox and Illingworth [32] for nonprecipitating marine stratocumulus clouds as $\mathrm{CER} = 46.7Z^{0.177}$. As shown in Fig. 8, the exponential relationship fit by our method from 2223 samples during the entire IOPs is $\mathrm{CER_{Ret}} = 27.4Z^{0.154}$. The fit coefficients (i.e., 27.4 and 0.154) are both in good agreement with the empirical coefficients for nonprecipitation clouds. The red solid line fit by our method is closer to the aircraft in situ data fit line (as shown by the gray solid line) than that of other traditional empirical methods. Especially for the large particles with reflectivity greater than −15 dBZ, our method can substantially alleviate the underestimation induced by traditional empirical algorithms. In addition, it should be noted that the CER$_{\mathrm{Ret}}$ fit coefficients discussed here are only used for evaluating our method rationality and are not a component of the method.

To further account for how the method error is affected by different variables, we investigate the fractional error between CER$_{\mathrm{Ret}}$ and CER$_{\mathrm{FCDP}}$ in each bin with width of 0.5 μm,

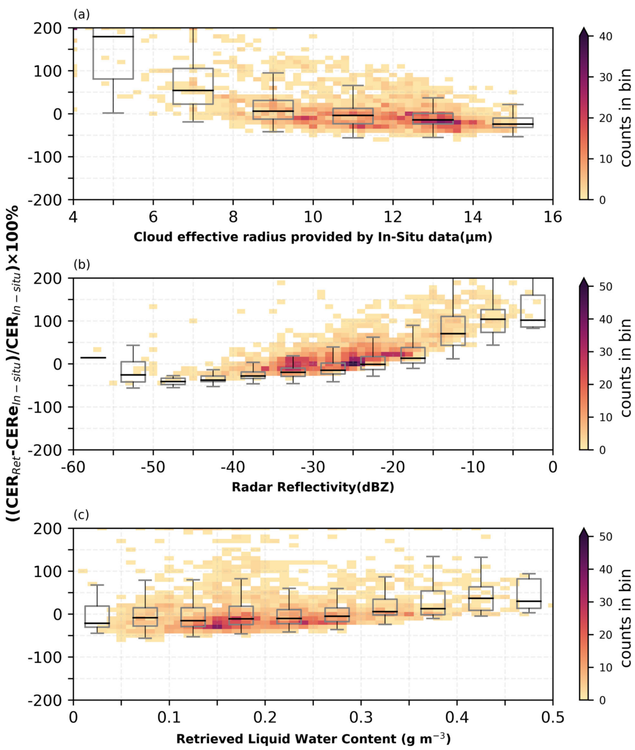

Fig. 9. Distribution of $\mathrm{CER_{Ret}}$ fractional errors corresponding to (a) CER provided by in situ data, (b) radar measured reflectivity factor, and (c) retrieved cloud LWC. The shaded area represents the sample number within the 10% $\mathrm{CER_{Ret}}$ fractional error on the vertical coordinate and the 0.5 μm, 1 dBZ, and 0.01 $\mathrm{g\,m^{-3}}$ bins in cloud particle size, radar reflectivity factor, and retrieved LWC on the horizontal coordinate, respectively. The gray boxplots in three different subgraphs represent the distribution of fractional error within 4 μm, 5 dBZ, and 0.5 $\mathrm{g\,m^{-3}}$ bins of $\mathrm{CER_{FCDP}}$, radar reflectivity, and retrieved LWC, respectively.

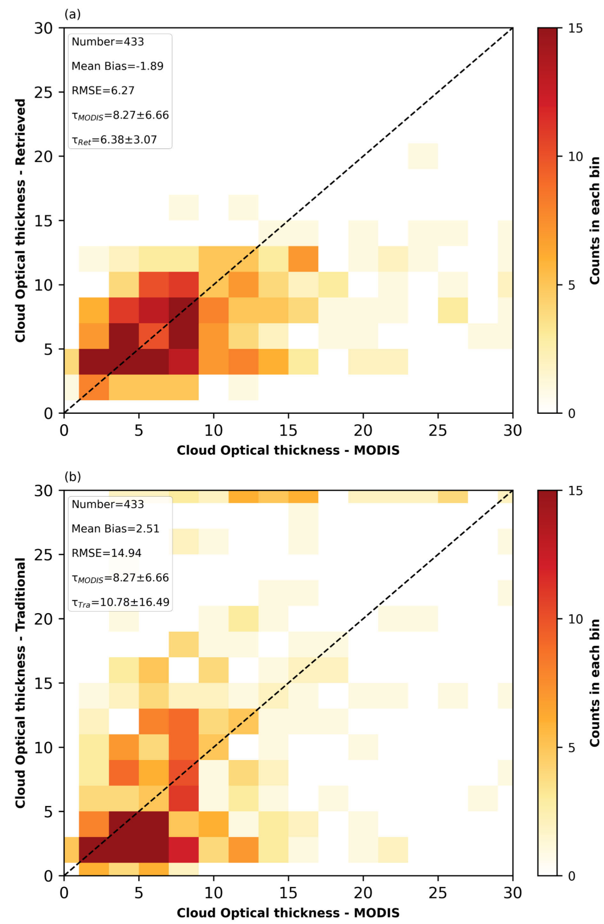

Fig. 10. Two-dimensional joint histograms of the COT retrieved by (a) our method and (b) traditional empirical method versus the MODIS products over the one year from June 2017 to May 2018. The number of samples in each bin with a width of 2 is displayed in different colors. More samples are represented by darker color and vice versa by a lighter color.

1 dBZ, and 0.01 $\mathrm{g\,m^{-3}}$ for CER, Z_m, and LWC, respectively, as shown in Fig. 9. Fig. 9(a) illustrates that the retrieval error is approximately zero corresponding to the CER within the range of 6–14 μm where the cloud droplet size is concentrated. Moreover, there are no obvious error variations with the increase of CER, confirming that the retrieval errors are independent of the particle size and are rarely affected by large particles. In addition, the retrieval errors are insignificantly affected by the reflectivity factor variation, especially for the nonprecipitation cloud with reflectivity lower than −15 dBZ, as shown in Fig. 9(b). There is a slight increase in error quartiles when the reflectivity factor falls within the range of −15 and −5 dBZ. This may be attributed to the fact that the aircraft in situ data are limited to the cloud droplet size, whereas the radar detects some large particles in this reflectivity range. Similarly, the fractional errors are also impervious to the variations in cloud LWC as depicted in Fig. 9(c), validating that the critical advantage of our method is that it is rarely constrained by variables and has robust stability.

V. Application of Algorithm in COT Retrieval

Since the CER is also a fundamental variable that determines cloud optical properties, it would be a convincing perspective to further verify the method's accuracy by calculating the optical properties from the retrieved CER. In this study, we attempt to estimate the COT (τ) from the retrieved CER by the following equation as [60]:

$$\tau = \frac{3}{2}\frac{\mathrm{LWP}}{\rho_w r_e} \tag{13}$$

where ρ_w is the density of liquid water about 1 $\mathrm{g\,m^{-3}}$ and LWP is the vertical integration of LWC in unit of $\mathrm{g\,m^{-2}}$. In accordance with Section III, $\mathrm{CER_{Ret}}$ can be calculated within each radar gate rather than the average value spanning the entire cloud layer. Therefore, the COT for the whole cloud layer has to be derived by the integration of (14) from CBH to CTH [i.e., $\tau = \sum_{j=\mathrm{CBH}}^{j=\mathrm{CTH}} \tau(h_j)$], where (14) is the COT in the ith radar gate discretized from (13) as expressed by

$$\tau(h_i) = \frac{3}{2}\frac{\mathrm{LWP}(h_i)}{r_e(h_i)} = \frac{3}{2}\frac{\mathrm{LWC}(h_i)\Delta s}{r_e(h_i)} \tag{14}$$

where Δs is the height between the adjacent radar gates in the vertical direction. In this study, Δs is equal to the cloud radar vertical resolution of 0.03 km, and the LWC in each radar gate are retrieved by the self-consistent method as detailed in Section III.

We retrieved the COT (hereafter COT_{Ret}) for a total of 433 instantaneous samples of single-layer clouds from June 2017 to May 2018 and compared it with the prevailing MODIS products during the same periods. The 2-D histogram of COT_{Ret} and that of the traditional empirical method (hereafter COT_{Tra}) versus the COT products provided by MODIS (hereafter COT_{MODIS}) are shown in Fig. 10, where COT_{Tra} is calculated from CER_{Tra}. COT_{Ret} is concentrated around the diagonal, while COT_{Tra} is distributed above the diagonal with significant overestimation compared to COT_{MODIS}. This can be attributed to a substantial underestimation in the traditional empirical method for CER retrieval in contrast to our method. The MBs in COT_{Ret} (6.38 ± 3.07) and COT_{Tra} (10.78 ± 16.49) are -1.89 and 2.51 compared to COT_{MODIS} (8.27 ± 6.66). The RMSE of COT_{Ret} is notably smaller than that of COT_{Tra}, i.e., 6.27 versus 14.94. The superb applicability of our method in COT retrieval and the reduction of overestimation caused by traditional empirical algorithms are effectively demonstrated.

VI. Conclusion

The main purpose of the work is to propose a CER retrieval method for single-wavelength radar based on the connections between CER, Z, and LWC under the assumption that cloud DSD follows the lognormal distribution. The cloud droplet number concentration is effectively eliminated by combining the Z and LWC definitions. Only one cloud DSD parameter r_m, which has been proved to have less influence on the retrieved CER, is given as constant through the sensitivity analysis. Innovatively, the LWC is obtained from the self-consistent algorithm constructed by the radiative transfer theory, and the measured reflectivity is attenuation corrected by utilizing the proportional relationship between absorption attenuation and LWC in this study. This ensures that this method can be applied to nonprecipitation and clouds with large particle sizes without relying on other instruments and empirical coefficients. Moreover, the uncertainty of our CER retrieval method is limited to only 15.3%, which is smaller than that of the uncertainty of the joint algorithm combining cloud radar and MWR.

The application of the algorithm in ground-based radar deployed at the ENA site, as well as the matching of radar and aircraft data, is demonstrated separately using two distinct cases that occurred on June 30, 2017, and January 29, 2018. The algorithm accuracy was evaluated by comparing CER_{Ret} with CER_{Tra} and CER_{FCDP} within 10 km from the site during the summer, winter, and entire IOPs, respectively. The results showed that the frequency distribution and vertical structure of CER_{Ret} and the curves fit by CER_{Ret} with Z are all in good alignment with that of the CER_{FCDP} compared to CER_{Tra} and CER_{σ}. The retrieval error is concentrated near zero and is less affected either by variations in droplet size, reflectivity factor, or cloud LWC. Furthermore, it is demonstrated that this method can be applied to calculate COT with smaller MB and RMSE than the traditional empirical algorithm by comparison with MODIS products.

In conclusion, the CER retrieval method constructed based on the self-consistent LWC algorithm, attenuation corrected reflectivity, and parameter r_m demonstrates lower uncertainty and higher accuracy compared to the traditional empirical coefficient algorithm and the algorithm with constant σ_x. Moreover, it proves to be applicable to retrieve other cloud optical properties by taking COT as an example. The CER retrieval method can be flexibly applied to ground-based and spaceborne single-wavelength cloud radar since it is constructed based on the principle of radar observation. Future work will focus on applying this method to spaceborne millimeter wavelength cloud radar, such as the cloud profiling radar (CPR) onboard CloudSat. This endeavor aims to modify this novel algorithm capable of retrieving LLCs' microphysical properties, including LWC, CER, and COT over a broad area. Although the algorithm is inevitably limited to the liquid water cloud and the parameter in cloud DSD is assumed to be constant, it may help to improve the characterization of LLCs properties in models and enhance the accuracy of climate predictions.

Acknowledgment

The authors are grateful to the Atmospheric Radiation Measurement (ARM) for the support of the ground-based and aircraft in situ data used in this study (www.arm.gov).

References

[1] I. Tan, T. Storelvmo, and M. D. Zelinka, "Observational constraints on mixed-phase clouds imply higher climate sensitivity," *Science*, vol. 352, no. 6282, pp. 224–227, Apr. 2016, doi: 10.1126/science.aad5300.

[2] M. D. Zelinka, I. Tan, L. Oreopoulos, and G. Tselioudis, "Detailing cloud property feedbacks with a regime-based decomposition," *Climate Dyn.*, vol. 60, nos. 9–10, pp. 2983–3003, May 2023, doi: 10.1007/s00382-022-06488-7.

[3] J. Ge, C. Zheng, H. Xie, Y. Xin, J. Huang, and Q. Fu, "Midlatitude cirrus clouds at the SACOL site: Macrophysical properties and large-scale atmospheric states," *J. Geophys. Res., Atmos.*, vol. 123, no. 4, pp. 2256–2271, Feb. 2018, doi: 10.1002/2017jd027724.

[4] H. Shang et al., "A hybrid cloud detection and cloud phase classification algorithm using classic threshold-based tests and extra randomized tree model," *Remote Sens. Environ.*, vol. 302, Mar. 2024, Art. no. 113957, doi: 10.1016/j.rse.2023.113957.

[5] G. L. Stephens, "Cloud feedbacks in the climate system: A critical review," *J. Climate*, vol. 18, no. 2, pp. 237–273, Jan. 2005, doi: 10.1175/jcli-3243.1.

[6] S. Koseki, T. Nakamura, H. Mitsudera, and Y. Wang, "Modeling low-level clouds over the Okhotsk Sea in summer: Cloud formation and its effects on the Okhotsk high," *J. Geophys. Res., Atmos.*, vol. 117, no. D5, Mar. 2012, Art. no. 2011JD016462, doi: 10.1029/2011jd016462.

[7] I. Koren, J. V. Martins, L. A. Remer, and H. Afargan, "Smoke invigoration versus inhibition of clouds over the Amazon," *Science*, vol. 321, no. 5891, pp. 946–949, Aug. 2008, doi: 10.1126/science.1159185.

[8] X. Zeng et al., "The radiative effect on cloud microphysics from the Arctic to the tropics," *Bull. Amer. Meteorological Soc.*, vol. 103, no. 9, pp. E2108–E2129, Mar. 2022, doi: 10.1175/bams-d-21-0039.1.

[9] H. Letu et al., "Surface solar radiation compositions observed from Himawari-8/9 and Fengyun-4 series," *Bull. Amer. Meteorol. Soc.*, vol. 104, no. 10, pp. E1772–E1789, Oct. 2023, doi: 10.1175/bams-d-22-0154.1.

[10] Y. Chen, F. Ping, S. Zhou, X. Shen, and Y. Sun, "Influence of microphysical processes on the initiation of the mesoscale convective system of a rainstorm over Beijing," *Atmos. Res.*, vol. 254, Jun. 2021, Art. no. 105518, doi: 10.1016/j.atmosres.2021.105518.

[11] J. Mülmenstädt et al., "An underestimated negative cloud feedback from cloud lifetime changes," *Nature Climate Change*, vol. 11, no. 6, pp. 508–513, Jun. 2021, doi: 10.1038/s41558-021-01038-1.

[12] T. Andrews, J. M. Gregory, M. J. Webb, and K. E. Taylor, "Forcing, feedbacks and climate sensitivity in CMIP5 coupled atmosphere-ocean climate models," *Geophys. Res. Lett.*, vol. 39, no. 9, May 2012, Art. no. 2012GL051607, doi: 10.1029/2012gl051607.

[13] M. D. Zelinka et al., "Causes of higher climate sensitivity in CMIP6 models," *Geophys. Res. Lett.*, vol. 47, no. 1, Jan. 2020, Art. no. e2019GL085782, doi: 10.1029/2019gl085782.

[14] T. J. Garrett and C. Zhao, "Increased Arctic cloud longwave emissivity associated with pollution from mid-latitudes," *Nature*, vol. 440, no. 7085, pp. 787–789, Apr. 2006, doi: 10.1038/nature04636.

[15] J. Wang, C. Liu, M. Min, X. Hu, Q. Lu, and L. Husi, "Effects and applications of satellite radiometer 2.25-μm channel on cloud property retrievals," *IEEE Trans. Geosci. Remote Sens.*, vol. 56, no. 9, pp. 5207–5216, Sep. 2018, doi: 10.1109/TGRS.2018.2812082.

[16] C. Barthlott, A. Zarboo, T. Matsunobu, and C. Keil, "Importance of aerosols and shape of the cloud droplet size distribution for convective clouds and precipitation," *Atmos. Chem. Phys.*, vol. 22, no. 3, pp. 2153–2172, Feb. 2022, doi: 10.5194/acp-22-2153-2022.

[17] G. Tana et al., "Retrieval of cloud microphysical properties from Himawari-8/AHI infrared channels and its application in surface shortwave downward radiation estimation in the sun glint region," *Remote Sens. Environ.*, vol. 290, May 2023, Art. no. 113548, doi: 10.1016/j.rse.2023.113548.

[18] B. A. Albrecht, "Aerosols, cloud microphysics, and fractional cloudiness," *Science*, vol. 245, no. 4923, pp. 1227–1230, Sep. 1989.

[19] H. Shang et al., "An improved algorithm of cloud droplet size distribution from POLDER polarized measurements," *Remote Sens. Environ.*, vol. 228, pp. 61–74, Jul. 2019, doi: 10.1016/j.rse.2019.04.013.

[20] M. Zemp et al., "GCOS 2022 implementation plan," in *Proc. Global Climate Observing Syst. (GCOS)*, vol. 244, 2022, p. 85.

[21] F. Chang and Z. Li, "Estimating the vertical variation of cloud droplet effective radius using multispectral near-infrared satellite measurements," *J. Geophys. Res., Atmos.*, vol. 107, no. D15, Aug. 2002, Art. no. AAC-7, doi: 10.1029/2001jd000766.

[22] D. P. Donovan and A. C. A. P. van Lammeren, "Cloud effective particle size and water content profile retrievals using combined LiDAR and radar observations: 1. Theory and examples," *J. Geophys. Res., Atmos.*, vol. 106, no. D21, pp. 27425–27448, Nov. 2001, doi: 10.1029/2001jd900243.

[23] M. D. Alexandrov et al., "Liquid water cloud properties during the polarimeter definition experiment (PODEX)," *Remote Sens. Environ.*, vol. 169, pp. 20–36, Nov. 2015, doi: 10.1016/j.rse.2015.07.029.

[24] M. Saito et al., "An efficient method for microphysical property retrievals in vertically inhomogeneous marine water clouds using MODIS-CloudSat measurements," *J. Geophys. Res., Atmos.*, vol. 124, no. 4, pp. 2174–2193, Feb. 2019, doi: 10.1029/2018jd029659.

[25] N. J. King and G. Vaughan, "Using passive remote sensing to retrieve the vertical variation of cloud droplet size in marine stratocumulus: An assessment of information content and the potential for improved retrievals from hyperspectral measurements," *J. Geophys. Res., Atmos.*, vol. 117, no. D15, Aug. 2012, Art. no. 2012JD017896, doi: 10.1029/2012jd017896.

[26] R. Meneghini, H. Kumagai, J. R. Wang, T. Iguchi, and T. Kozu, "Microphysical retrievals over stratiform rain using measurements from an airborne dual-wavelength radar-radiometer," *IEEE Trans. Geosci. Remote Sens.*, vol. 35, no. 3, pp. 487–506, May 1997, doi: 10.1109/36.581956.

[27] D. Atlas, "The estimation of cloud parameters by radar," *J. Atmos. Sci.*, vol. 11, no. 4, pp. 309–317, Jan. 1954, doi: 10.1175/1520-0469(1954)011<0309:TEOCPB>2.0.CO;2.

[28] C. Zhao et al., "Toward understanding of differences in current cloud retrievals of ARM ground-based measurements," *J. Geophys. Res., Atmos.*, vol. 117, no. D10, p. 2011, May 2012, Art. no. 2011JD016792, doi: 10.1029/2011jd016792.

[29] N. Wood, "Level 2B radar-visible optical depth cloud water content (2B-CWC-RVOD) process description document," *Version*, vol. 5, pp. 1–26, Oct. 2008.

[30] G. G. Mace and K. Sassen, "A constrained algorithm for retrieval of stratocumulus cloud properties using solar radiation, microwave radiometer, and millimeter cloud radar data," *J. Geophys. Res., Atmos.*, vol. 105, no. D23, pp. 29099–29108, Dec. 2000, doi: 10.1029/2000jd900403.

[31] R. T. Austin and G. L. Stephens, "Retrieval of stratus cloud microphysical parameters using millimeter-wave radar and visible optical depth in preparation for CloudSat: 1. Algorithm formulation," *J. Geophys. Res., Atmos.*, vol. 106, no. D22, pp. 28233–28242, Nov. 2001, doi: 10.1029/2000jd000293.

[32] N. I. Fox and A. J. Illingworth, "The retrieval of stratocumulus cloud properties by ground-based cloud radar," *J. Appl. Meteorol. Climatol.*, vol. 36, no. 5, pp. 485–492, Aug. 1997, doi: 10.1175/1520-0450(1997)036<0485:TROSCP>2.0.CO;2.

[33] P. Wu, X. Dong, and B. Xi, "A climatology of marine boundary layer cloud and drizzle properties derived from ground-based observations over the Azores," *J. Climate*, vol. 33, no. 23, pp. 10133–10148, Dec. 2020, doi: 10.1175/jcli-d-20-0272.1.

[34] X. Dong, B. Xi, and P. Wu, "Investigation of the diurnal variation of marine boundary layer cloud microphysical properties at the Azores," *J. Climate*, vol. 27, no. 23, pp. 8827–8835, Dec. 2014, doi: 10.1175/jcli-d-14-00434.1.

[35] R. Wood, "Drizzle in stratiform boundary layer clouds. Part I: Vertical and horizontal structure," *J. Atmos. Sci.*, vol. 62, no. 9, pp. 3011–3033, Sep. 2005, doi: 10.1175/jas3529.1.

[36] J. Ge et al., "A novel liquid water content retrieval method based on mass absorption for single-wavelength cloud radar," *IEEE Trans. Geosci. Remote Sens.*, vol. 61, 2023, Art. no. 4102815, doi: 10.1109/TGRS.2023.3278735.

[37] J. I. Song, S. S. Yum, S. Park, K. Kim, K. Park, and S. Joo, "Climatology of melting layer heights estimated from cloud radar observations at various locations," *J. Geophys. Res., Atmos.*, vol. 126, no. 17, Sep. 2021, Art. no. e2021JD034816, doi: 10.1029/2021jd034816.

[38] K. Widener, N. Bharadwaj, and K. Johnson. (Mar. 2012). *Ka-Band ARM Zenith Radar (KAZR) Instrument Handbook*. DOE Office of Sci. Atmospheric Radiat. Meas. (ARM) Program. Accessed: Nov. 1, 2023. [Online]. Available: https://www.osti.gov/biblio/1035855

[39] I. Silber, J. Verlinde, G. Wen, and E. W. Eloranta, "Can embedded liquid cloud layer volumes be classified in polar clouds using a single- frequency zenith-pointing radar?" *IEEE Geosci. Remote Sens. Lett.*, vol. 17, no. 2, pp. 222–226, Feb. 2020, doi: 10.1109/LGRS.2019.2918727.

[40] E. E. Clothiaux et al., *The ARM Millimeter Wave Cloud Radars (MMCRs) and the Active Remote Sensing of Clouds (ARSCL) Value Added Product (VAP)*, document DOE/SC-ARM/VAP-002.1, DOE Office Sci. Atmos. Radiat. Meas. (ARM) User Facility, Mar. 2001.

[41] P. Kollias et al., "Development and applications of ARM millimeter-wavelength cloud radars," *Meteorological Monographs*, vol. 57, pp. 1–17, Apr. 2016, doi: 10.1175/AMSMONOGRAPHS-D-15-0037.1.

[42] J. Wang et al., "Aerosol and cloud experiments in the eastern North Atlantic (ACE-ENA)," *Bull. Amer. Meteorol. Soc.*, vol. 103, no. 2, pp. E619–E641, Feb. 2022, doi: 10.1175/bams-d-19-0220.1.

[43] B. Schmid et al., "The DOE ARM aerial facility," *Bull. Amer. Meteorol. Soc.*, vol. 95, no. 5, pp. 723–742, May 2014, doi: 10.1175/bams-d-13-00040.1.

[44] S. Glienke and F. Mei. (2020). *Fast Cloud Droplet Probe (FCDP) Instrument Handbook*. Pacific Northwest Nat. Lab, Oak Ridge, TN, USA. Accessed: Nov. 1, 2023. [Online]. Available: https://www.osti.gov/biblio/1597469

[45] M. D. Lebsock and M. Witte, "Quantifying the dependence of drop spectrum width on cloud drop number concentration for cloud remote sensing," *Atmos. Chem. Phys.*, vol. 23, no. 22, pp. 14293–14305, Nov. 2023, doi: 10.5194/acp-23-14293-2023.

[46] S. Platnick et al., "The MODIS cloud optical and microphysical products: Collection 6 updates and examples from Terra and Aqua," *IEEE Trans. Geosci. Remote Sens.*, vol. 55, no. 1, pp. 502–525, Jan. 2017, doi: 10.1109/TGRS.2016.2610522.

[47] X. Yang, J. Ge, X. Hu, M. Wang, and Z. Han, "Cloud-top height comparison from multi-satellite sensors and ground-based cloud radar over SACOL site," *Remote Sens.*, vol. 13, no. 14, p. 2715, Jul. 2021, doi: 10.3390/rs13142715.

[48] J. Ge, Z. Wang, Y. Liu, J. Su, C. Wang, and Z. Dong, "Linkages between mid-latitude cirrus cloud properties and large-scale meteorology at the SACOL site," *Climate Dyn.*, vol. 53, nos. 7–8, pp. 5035–5046, Jun. 2019, doi: 10.1007/s00382-019-04843-9.

[49] N. L. Miles, J. Verlinde, and E. E. Clothiaux, "Cloud droplet size distributions in low-level stratiform clouds," *J. Atmos. Sci.*, vol. 57, no. 2, pp. 295–311, Jan. 2000, doi: 10.1175/1520-0469(2000)057<0295:CDSDIL>2.0.CO;2.

[50] S. Frisch, M. Shupe, I. Djalalova, G. Feingold, and M. Poellot, "The retrieval of stratus cloud droplet effective radius with cloud radars," *J. Atmos. Ocean. Technol.*, vol. 19, no. 6, pp. 835–842, Jun. 2002, doi: 10.1175/1520-0426(2002)019<0835:TROSCD>2.0.CO;2.

[51] S. Yao, J. He, H. Wang, S. Tang, and X. Liang, "The attenuation correction for Ka band cloud radar," in *Proc. Int. Conf. Meteorol. Observat. (ICMO)*, Dec. 2019, pp. 1–4. Accessed: Nov. 1, 2023. [Online]. Available: https://ieeexplore.ieee.org/abstract/document/9025886/

[52] X. Zheng, B. Xi, X. Dong, P. Wu, T. Logan, and Y. Wang, “Environmental effects on aerosol–cloud interaction in non-precipitating marine boundary layer (MBL) clouds over the eastern North Atlantic,” *Atmos. Chem. Phys.*, vol. 22, no. 1, pp. 335–354, Jan. 2022, doi: 10.5194/acp-22-335-2022.

[53] P. Wu, X. Dong, B. Xi, J. Tian, and D. M. Ward, “Profiles of MBL cloud and drizzle microphysical properties retrieved from ground-based observations and validated by aircraft in situ measurements over the Azores,” *J. Geophys. Res., Atmos.*, vol. 125, no. 9, May 2020, Art. no. e2019JD032205, doi: 10.1029/2019jd032205.

[54] F. Gallo et al., “Long-range transported continental aerosol in the Eastern North Atlantic: Three multiday event regimes influence cloud condensation nuclei,” *Atmos. Chem. Phys. Discuss.*, vol. 27, no. 3, pp. 1–27, 2022, doi: 10.5194/acp-23-4221-2023.

[55] R. Wood et al., “Clouds, aerosols, and precipitation in the marine boundary layer: An arm mobile facility deployment,” *Bull. Amer. Meteorol. Soc.*, vol. 96, no. 3, pp. 419–440, Mar. 2015, doi: 10.1175/bams-d-13-00180.1.

[56] X. Dong, B. Xi, A. Kennedy, P. Minnis, and R. Wood, “A 19-month record of marine aerosol–cloud–radiation properties derived from DOE ARM mobile facility deployment at the azores. Part I: Cloud fraction and single-layered MBL cloud properties,” *J. Climate*, vol. 27, no. 10, pp. 3665–3682, May 2014, doi: 10.1175/jcli-d-13-00553.1.

[57] T. Kobayashi, “Significant differences in the cloud droplet effective radius between nonprecipitating and precipitating clouds,” *Geophys. Res. Lett.*, vol. 34, no. 15, Aug. 2007, Art. no. 2007GL029606, doi: 10.1029/2007gl029606.

[58] Y. Chen et al., “Retrieval of the vertical evolution of the cloud effective radius from the Chinese FY-4 (Feng yun 4) next-generation geostationary satellites,” *Atmos. Chem. Phys.*, vol. 20, no. 2, pp. 1131–1145, Jan. 2020, doi: 10.5194/acp-20-1131-2020.

[59] H. Sauvageot and J. Omar, “Radar reflectivity of cumulus clouds,” *J. Atmos. Ocean. Technol.*, vol. 4, no. 2, pp. 264–272, Jun. 1987, doi: 10.1175/1520-0426(1987)004<0264:RROCC>2.0.CO;2.

[60] G. L. Stephens, “Radiation profiles in extended water clouds. II: Parameterization schemes,” *J. Atmos. Sci.*, vol. 35, no. 11, pp. 2123–2132, Nov. 1978.

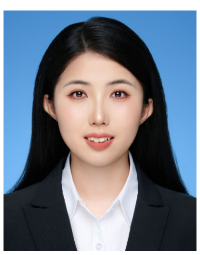

Jiajing Du received the B.S. degree in atmospheric science from Lanzhou University, Lanzhou, China, in 2019, where she is currently pursuing the Ph.D. degree.

Her research interests include radar data processing and cloud physical properties’ retrieval algorithm.

Jinming Ge received the B.S. and Ph.D. degrees in atmospheric science from Lanzhou University, Lanzhou, China, in 2005 and 2010, respectively.

From 2010 to 2012, he was a Lecturer with Lanzhou University, where he became an Associate Professor in 2012 and has been a Professor since 2017. He is currently the Professor with the Key Laboratory for Semi-Arid Climate Change of the Ministry of Education and College of Atmospheric Sciences, Lanzhou University. His research interests include atmosphere aerosols, cloud physical properties retrieval, and their radiative effects on climate.

Chi Zhang received the B.S. degree in atmospheric science from Chengdu University of Information Technology, Chengdu, China, in 2021. He is currently pursuing the Ph.D. degree with Lanzhou University, Lanzhou, China.

His research interests include millimeter-wave radar data processing and its application in studying diurnal variations of clouds.

Jing Su received the B.S. and Ph.D. degrees in atmospheric science from Lanzhou University, Lanzhou, China, in 2005 and 2010, respectively.

She is currently an Associate Professor with the Key Laboratory for Semi-Arid Climate Change of the Ministry of Education and College of Atmospheric Sciences, Lanzhou University. Her research interests include the physical properties of cloud and dust aerosols and their radiation effects.

Xiaoyu Hu received the Ph.D. degree in atmospheric science from Lanzhou University, Lanzhou, China, in 2022.

He is currently a Post-Doctoral Researcher at Chongqing Research Institute of Big Data, Peking University, Beijing, China. His research interests include cloud remote sensing and artificial intelligence application.

Zeen Zhu received the M.S. degree in atmospheric science from Lanzhou University, Lanzhou, China, in 2017, and the Ph.D. degree in atmospheric science from Stony Brook University, Stony Brook, NY, USA, in 2022.

He is currently a Research Associate with Brookhaven National Laboratory and has been a Graduate Research Assistant with the School of Marine and Atmospheric Science, Stony Brook University, since 2017. His research interests include cloud remote sensing and radar applications.

Qinghao Li received the B.S. degree from Lanzhou University, Lanzhou, China, in 2019, where he is currently pursuing the Ph.D. degree.

His research interests include aerosol–cloud interaction and its influence on radiation.

Jianping Huang received the Ph.D. degree in weather dynamics from Lanzhou University, Lanzhou, China, in 1988.

He performed a post-doctoral work with Peking University, Beijing, China. He is an Academician at Chinese Academy of Sciences, Beijing, and a Professor at the Key Laboratory for Semi-Arid Climate Change of the Ministry of Education and the College of Atmospheric Sciences, Lanzhou University. He is the main author of the first working group of Working Group I of the Fifth Assessment Report of the Intergovernmental Panel on Climate Change (IPCC) and is one of the academic leaders in the field of atmospheric science in China who has combined systematic observation and theoretical research and made major breakthroughs. He plays an important role in semi-arid climate research in China. He created and developed the first semi-arid climate comprehensive observation station with international standards in western China. His research interests include the global arid and semi-arid regions and the interaction of dust aerosols with clouds and precipitation.

Qiang Fu received the B.S. and M.S. degrees in atmospheric physics from Peking University, Beijing, China, in 1983 and 1986, respectively, and the Ph.D. degree in atmospheric science from the University of Utah, Salt Lake City, UT, USA, in 1991.

He is currently an Academician at the National Academy of Sciences and a Professor of atmospheric sciences at the University of Washington, Seattle, WA, USA. His research interests include light scattering and radiative transfer, atmospheric radiation and clouds, atmospheric aerosols, remote sensing, climate, and climate change.